DIAB, M.R., MURASAWA, K., WANG, M., OHMAGARI, S., NARAGINO, H., YOSHITAKE, T. and EGIZA, M. 2025. Unveiling the durability, friction, and wear behaviour of nanodiamond composite films deposited on biased cemented carbide with varying Al interlayer thickness. *Surfaces and interfaces* [online], 63, article number 106367. Available from: https://doi.org/10.1016/j.surfin.2025.106367

Unveiling the durability, friction, and wear behaviour of nanodiamond composite films deposited on biased cemented carbide with varying Al interlayer thickness.

DIAB, M.R., MURASAWA, K., WANG, M., OHMAGARI, S., NARAGINO, H., YOSHITAKE, T. and EGIZA, M.

2025

Surfaces and Interfaces 63 (2025) 106367

Contents lists available at ScienceDirect

Surfaces and Interfaces

journal homepage: www.sciencedirect.com/journal/surfaces-and-interfaces

Unveiling the durability, friction, and wear behaviour of nanodiamond composite films deposited on biased cemented carbide with varying Al interlayer thickness

Mohamed Ragab Diab [a,b,*], Koki Murasawa [a,c], Mei Wang [c], Shinya Ohmagari [d], Hiroshi Naragino [a], Tsuyoshi Yoshitake [a,*], Mohamed Egiza [b,e,*]

[a] Department of Advanced Energy Science and Engineering, Faculty of Engineering Sciences, Kyushu University, Kasuga, Fukuoka 816-8580, Japan
[b] Department of Mechanical Engineering, Kafrelsheikh University, Kafrelsheikh, 33516, Egypt
[c] OSG Corporation, 3-22 Honnogahara, Toyokawa, Aichi 442-8543, Japan
[d] Sensing System Research Center, National Institute of Advanced Industrial Science and Technology (AIST), 807-1 Shuku-machi, Tosu, Saga, 841-0052, Japan
[e] School of Computing, Engineering and technology, Robert Gordon University, Aberdeen, AB107GJ, UK

ARTICLE INFO

Keywords:
Nanocomposite coatings
Coaxial arc plasma deposition
Al interlayer
Co catalytic effect
Adhesion strength
Wear resistance

ABSTRACT

Nanodiamond composite (NDC) films were deposited on biased cemented carbide (WC−6 wt. % Co) substrates using a coaxial arc plasma deposition technique, incorporating sputtered aluminium (Al) interlayers with varying thicknesses (0,50, 100, 300, and 500 nm). This study systematically investigates the durability, friction, and wear behaviour of NDC films, focusing on optimizing Al interlayer thickness to enhance performance in dry and harsh machining conditions. The primary objective was to mitigate interfacial catalytic reactions, particularly Co-induced graphitization, which adversely affect adhesion and mechanical integrity. Experimental findings identified a 100 nm Al interlayer as the optimal configuration, forming a protective Al_2O_3 layer that effectively suppressed graphitization. This resulted in significant improvements in coating performance, including a 79 % increase in adhesion strength, as indicated by a critical load of 17 N for full spallation during scratch testing, and a 62 % enhancement in wear resistance, yielding a wear rate of 7.85×10^{-8} mm^3/N.m. Simultaneously, the coefficient of friction (COF) decreased by 71 % compared to the uncoated substrate, maintaining a stable value of 0.09 during dry sliding tests against a rough Al_2O_3 counterpart. The exceptional tribological performance of the optimized NDC coatings is attributed to multiple factors. The refined nanostructure, featuring a dense grain boundary network, facilitated the formation of a lubricating graphitic layer, contributing to low and stable friction. Additionally, the high hardness (75 GPa) and Young's modulus (724 GPa) provided superior wear resistance and load-bearing capacity. These results underscore the potential of Al interlayers to significantly enhance the tribological performance of NDC coatings. However, the improvements in durability remain limited by the low adhesion strength, which remains a critical factor for cutting tools operating under dry machining conditions.

1. Introduction

Machining remains a cornerstone in the manufacturing of diverse components across various industries [1]. Cemented carbide tools, particularly those composed of tungsten carbide (WC) with a cobalt (Co) binder (WC−Co), are widely employed due to their exceptional wear resistance, hardness, and chemical stability compared with high speed steel tools [2]. This combination of properties translates to extended tool life and reliable performance in a multitude of machining applications [3].

The shift towards sustainable manufacturing has reduced reliance on cutting fluids, promoting dry machining techniques [4,5]. Unfortunately, dry machining, especially at high cutting speeds, exposes the cutting tool to severe tribological conditions and significant thermal stress on the tool surface, particularly the rake face [6,7]. The rapid wear of tools in dry machining environments leads to frequent replacements, reducing production efficiency and increasing costs, ultimately compromising tool durability.

---

* Corresponding authors.
E-mail addresses: mohamed.diab@kyudai.jp (M.R. Diab), Tsuyoshi_yoshitake@kyudai.jp (T. Yoshitake), Mohamed_Egiza@eng.kfs.edu.eg (M. Egiza).

https://doi.org/10.1016/j.surfin.2025.106367
Received 21 September 2024; Received in revised form 14 February 2025; Accepted 31 March 2025

Cutting tool durability, a critical parameter for successful machining operations, is influenced by a multitude of factors, including substrate material, tool geometry, micro-geometry, and the presence of thin-film coatings [8]. Optimizing cutting performance and achieving high productivity necessitate a comprehensive consideration of these factors. Thin-film coatings, particularly those exhibiting high hardness, wear resistance, low friction, and strong adhesion, play a pivotal role in enhancing tool life and overall machining efficiency.

To improve tool performance and mitigate the challenges of dry machining, protective coatings are commonly applied [9]. Over 90 % of cemented carbide tools currently utilize various coating techniques, such as chemical vapor deposition (CVD) or physical vapor deposition (PVD) [10]. Among these, CVD diamond coatings stand out due to their superior hardness and wear resistance, making them well-suited for machining challenging materials like carbon plastics, graphite, and aluminum-silicon alloys [11–13].

However, a significant challenge with diamond coatings lies in the Co-induced graphitization that can occur during the growth process due to the catalytic effect of cobalt in the WC−Co substrate [14]. This catalytic effect facilitates the transformation of strong sp^3 bonds, characteristic of diamond, into weaker sp^2 bonds, characteristic of graphite, at the coating-substrate interface. This transformation reduces the adhesion strength of the coating, leading to less durable coatings that require frequent tool replacements, thereby increasing the total machining cost. Additionally, a significant thermal mismatch exists between diamond coatings and the WC−Co substrate, further compromising adhesion strength and thus durability.

One approach to address this issue involves removing the Co from substrate surface through harsh techniques like acid etching and pulsed laser ablation. However, these methods often compromise the substrate's integrity by causing tissue loss on the surface layer, ultimately impacting the fracture strength of the coated tool [15]. Researchers have explored a more promising alternative: incorporating a thin metallic interlayer between the diamond coating and the WC−Co base. This interlayer acts as a barrier, suppressing the unwanted interaction between carbon and Co during deposition. Ideally, the chosen interlayer material should have two key properties. First, it needs a coefficient of thermal expansion that bridges the gap between diamond coating and WC−Co, minimizing the stress caused by temperature fluctuations. Second, it should effectively restrict Co diffusion by either confining it within the substrate or forming stable compounds with it. This prevents Co from reaching the coating and hindering the detrimental transformation to graphite [16,17].

While various metals such as titanium, molybdenum, and chromium have been explored as interlayers [18–21], aluminum (Al) presents unique advantages including low cost, availability, and ease of deposition [22–24]. It was reported that a thin Al interlayer significantly improves diamond coating adhesion on diverse substrates like steel, copper, and WC−Co [25,26]. This enhanced adhesion is attributed to the formation of an amorphous aluminum oxide layer during deposition, effectively suppressing cobalt diffusion. Additionally, Al is believed to interact with transition metals like Co, further reducing their catalytic impact on graphitization. Despite concerns about Al's fragility during pre-treatment stages [25–28], it remains a promising interlayer material for diamond coatings due to its ability to both reduce Co diffusion/graphitization and improve adhesion between the coating and the substrate.

Nanodiamond composite (NDC) coatings are emerging as a strong alternative to traditional diamond coatings for dry machining applications [13,29]. These coatings combine the exceptional properties of diamond coatings such as high hardness and thickness with the advantages of an amorphous carbon such as smooth surface and low coeffecient of friction (COF), making them ideal for dry machining environments where cutting fluids are not used or when minimal quantity of lubricants are employed [30,31]. CAPD is an eco-friendly PVD technique that creates dense and superhard NDC films with a high proportion of diamond-like sp^3-bonded carbon atoms [32,33]. This method is attractive because it doesn't require high temperatures or harsh chemical etching of the cobalt (Co) in WC−Co substrates, minimizing environmental impact [34].

While NDC coatings offer numerous benefits, previous research has shown a trade-off when employing negative bias voltage during CAPD deposition [35–37]. Applying negative bias undoubtedly augments the coating's hardness and densification, thereby engendering enhanced wear resistance. Nevertheless, this advantageous outcome is accompanied by a substantial diminution of adhesion between the NDC film and the cemented carbide substrate [36]. Given the established advantages of Al interlayers in improving adhesion of diamond coatings and the potential benefits of negative bias voltage for NDC films, a gap exists in the current research.

This study aims to explore the durability, friction, and wear performance of NDC coatings for dry machining applications. It examines the influence of varying Al interlayer thicknesses (0,50, 100, 300, and 500 nm) on the mechanical and tribological properties of NDC coatings deposited on biased cemented carbide substrates. This research aims to optimize Al interlayer thickness to achieve low-friction and wear-resistant coatings with enhanced interfacial adhesion strength suitable for harsh operating environments.

2. Experimental methods

2.1. Materials and films preparations

WC−Co plates, with a diameter of 10 mm, thickness of 5.5 mm, and 6 wt. % cobalt content, served as the substrate for film deposition due to their balance of hardness and toughness. WC−Co pin-shaped samples with coated spherical ends (6 mm in diameter, 20 mm in length) were prepared for tribological testing using the pin-on-disk method. Polished alumina (Al_2O_3) disks (20 mm in diameter, 3 mm thick) were used as the counter-body material in friction tests, providing a standardized, wear-resistant surface.

Prior to Al interlayer sputtering, WC−Co substrates underwent a cleaning process to ensure optimal adhesion. This included chemical roughening to create a controlled surface texture (Ra: 100 ± 10 nm) for better mechanical interlocking, followed by ultrasonic cleaning with acetone, methanol, and ultrapure water (5 min each). The sonication process removed contaminants, paving the way for strong film adhesion.

An Al interlayer was prepared using DC sputtering with a high-purity aluminium (99.9 wt. %) target. The deposition occurred at room temperature with a DC power supply set to 370 V. Pre-sputtering, the target surface underwent plasma cleaning with argon gas at 5 sccm for 5 min. The substrate-target distance was 70 mm, and the deposition rate was 27 nm/min, allowing for interlayer thicknesses of 50, 100, 300, and 500 nm.

NDC coatings were deposited onto the WC−Co substrates utilizing PVD-CAPD apparatus with a ULVAC APG-1000 arc gun as depicted in Fig. 1. The system operated at a base pressure of 5×10^{-5} Pa, with a discharge voltage of 100 V, no external heating, a target−substrate distance (TSD) of 15 mm, and a repetition rate of 1 Hz. A DC bias power supply applied at −100 V with a frequency of 40 kHz and a 35 % duty cycle to the substrate holder. This process allowed direct deposition of NDC coatings with 3 μm ± 0.5 μm film thickness at room substrate-temperature, eliminating the need for diamond seeding or Co removal, as often required in CVD diamond film growth, thus offering greater efficiency and broader applicability for NDC coatings. To confirm reproducibility, the film deposition process was repeated, and the deposited films were reanalysed to verify consistency in structural, mechanical, and tribological properties.

2.2. Films characterization

Various techniques were employed to comprehensively characterize

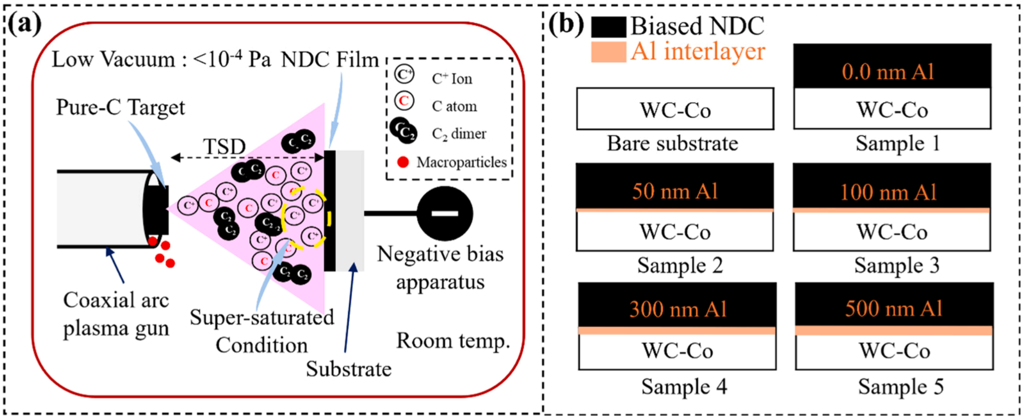

Fig. 1. (Colour online) (a) Schematic diagram of coaxial arc plasma deposition (CAPD) technique and (b) Experimental design for NDC coatings with 0 : 500 nm Al interlayers, compared to the bare substrate.

the fabricated NDC coatings. Morphological and nanostructural features were investigated using field emission scanning electron microscopy (FE-SEM, JEOL JSM-IT700HR). This high-resolution imaging technique provided detailed information on the surface features and morphology of the coatings at the nanoscale. Additionally, a 3D laser microscope (LEXT OLS5000, Olympus) was utilized to generate a three-dimensional profile of the film surface, quantifying its overall topography. Visible Raman spectroscopy (532 nm laser, Alpha 300R-confocal, Witec, Germany) was employed to elucidate the chemical composition and bonding configurations within the NDC films. Furthermore, the structural investigation of Al interlayer was performed by the XRD technique (SmartLab X-ray diffractometer, Rigaku Corp., Japan).

The mechanical properties of the coatings, particularly hardness and adhesion strength, were assessed. The hardness of the NDC films was determined through the implementation of nanoindentation testing, utilizing the Picodentor HM500 apparatus (Fischer Inst. UK) assembled with a Berkovich diamond indenter. This technique offers precise control over the applied force and displacement on the film surface at room temperature. A maximum load of 5.0 mN was applied with a defined loading and holding time profile (5.0 mN/10 s and 5 s, respectively) to ensure consistent measurements. Multiple indentations (15 points) were performed on randomly chosen locations across the surface for robust data analysis. To evaluate the adhesion strength between the films and the WC−Co substrates, scratch tests (Anton Paar RST^3) and the Rockwell D (load = 100 kg) indentation test were conducted. These tests assess the films' resistance to mechanical removal or delamination from the underlying substrate.

Finally, the tribological properties, specifically wear resistance, were investigated using a pin-on-disk tribometer (FPR-2000) under ambient conditions (open air, 50 % relative humidity) without lubrication. A pin-shaped NDC coated sample was loaded against a stationary alumina (Al_2O_3) disk with a normal load of 3.0 N, resulting in a contact pressure of approximately 3.0 GPa [38]. The test parameters included a controlled rotation diameter (10 mm) and linear speed (20 cm/s) to simulate wear conditions. The coefficient of friction between the pin and the disk was continuously monitored throughout the test. The wear resistance of the NDC coatings was then evaluated using the Archard equation based on the measured wear track dimensions [39]. Following the wear tests, FE-SEM, 3D laser microscopy, and Raman spectroscopy were again employed to analyze the wear tracks on the NDC samples. This post-wear analysis aimed to identify the wear morphologies, formation of tribo-films (transfering layers generated during wear), and any potential changes in the chemical composition of the worn surfaces.

3. Results and discussion

3.1. Nanoindentation measurements

Hardness (H) and Young's modulus (E) are critical parameters for assessing the mechanical performance and durability of NDC films for practical applications. Fig. 2 presents the evolution of these properties for biased NDC coatings deposited with varied Al interlayer thickness (0,50, 100, 300, and 500 nm). The application of a negative substrate biasing voltage (−100 V) during deposition markedly improved the mechanical properties of NDC coatings, achieving hardness and Young's modulus values of 70.8 GPa and 759.7 GPa, respectively, compared to 51.3 GPa and 516 GPa for unbiased coatings [32]. This demonstrates a 38 % increase in hardness and a 47 % improvement in Young's modulus due to substrate biasing, along with a 221 % increase in hardness compared to the bare WC−Co substrate ($H = 22$ GPa, $E = 527$ GPa). The improved mechanical properties can be attributed to the effective acceleration of positively charged carbon species (C^+) under the negative substrate bias, which, upon deceleration at the substrate surface, promotes denser film growth and a more robust microstructure, enhancing both hardness and Young's modulus [40].

When an Al interlayer was introduced with varying thicknesses (50–500 nm), hardness increased gradually for NDC coatings with 50 nm and 100 nm layers but decreased for those with 300 nm and 500 nm interlayers. Additionally, Young's modulus reached its highest value at a 50 nm Al interlayer and then gradually decreased as the interlayer thickness increased. The trend observed in hardness and Young's modulus suggests that a 50 nm Al interlayer is insufficient for the complete suppression of catalytic effects of cobalt at the interface. Consequently, a 100 nm Al interlayer is identified as the optimal thickness for achieving the highest hardness and improved mechanical performance. However, the maximum hardness achieved with a 100 nm Al interlayer in previous study was limited at 58 GPa [34].

In the present study, the introduction of a 100 nm thick Al interlayer before depositing biased NDC films resulted in further interesting modifications to the mechanical properties. Hardness increased slightly to 75 GPa, representing a 5.9 % improvement in comparison with NDC coatings fabricated directly onto the substrate (70.8 GPa). Conversely, Young's modulus decreased to 724 GPa from 760 GPa, a reduction of approximately 4.7 %. This inverse relationship between hardness and Young's modulus is atypical, as these properties generally exhibit a positive correlation. The observed trend suggests that the inserted Al interlayers (100–500 nm) effectively block the Co catalytic effects at the interface, leading to noticeable changes in the film structure, particularly in the quality of the films' nanostructure.

The Al interlayer might play a dual role. First, it could enhance the mobility of atoms on the substrate surface, facilitating the acceleration

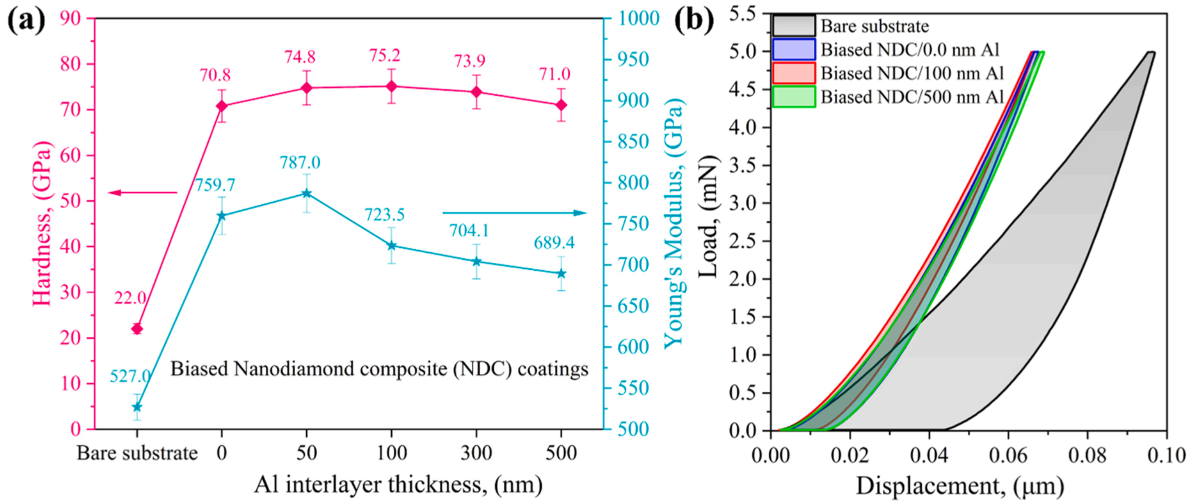

Fig. 2. (Colour online) (a) Nanoindentation test results of NDC coatings and (b) mean load–displacement curves for NDC coatings with 0.0, 100, and 500 nm Al interlayers, compared to the bare substrate.

of positively charged carbon species (C^{+}) during deposition with substrate biasing. This improved mobility might lead to denser film growth, contributing to the observed increase in hardness. Second, the Al interlayer could eliminate the Co catalytic effects at the interface between the film and the WC−Co substrate. Since cobalt is known to promote graphitization, which reduces film hardness, by suppressing this effect, the Al interlayer might indirectly contribute to enhanced hardness.

Nevertheless, an increase in the Al interlayer thickness, beyond a threshold of 100 nm, results in adverse mechanical properties being exhibited by NDC coatings. At 500 nm, hardness decreased to 71 GPa, and Young's modulus reduced to 689.4 GPa. The increased thickness of the Al interlayer to approximately 700 nm, relative to the actual Al interlayer thickness (500 nm) due to NDC deposition, apparently confirm the formation of an Al-carbide phase at the interface, as indicated in cross-sectional EDS analysis (refer to Figs. 4 and 10). The diffusion of soft Al atoms into the interface disrupts the film's structure, weakening its mechanical properties. These results suggest that a 100 nm Al interlayer provides an optimal balance, enhancing the mechanical properties of biased NDC films.

3.2. *Surface morphology and topography of NDC coatings*

Figs. 3 and 4 presents top-view and cross-sectional FE-SEM/ EDS mapping images of the deposited NDC films without and with 100 and 500 nm Al interlayers. The images reveal dense film structures devoid of pores and related defects, which are characteristic artifacts associated with the PVD deposition methods [41]. The film growth on the WC−Co

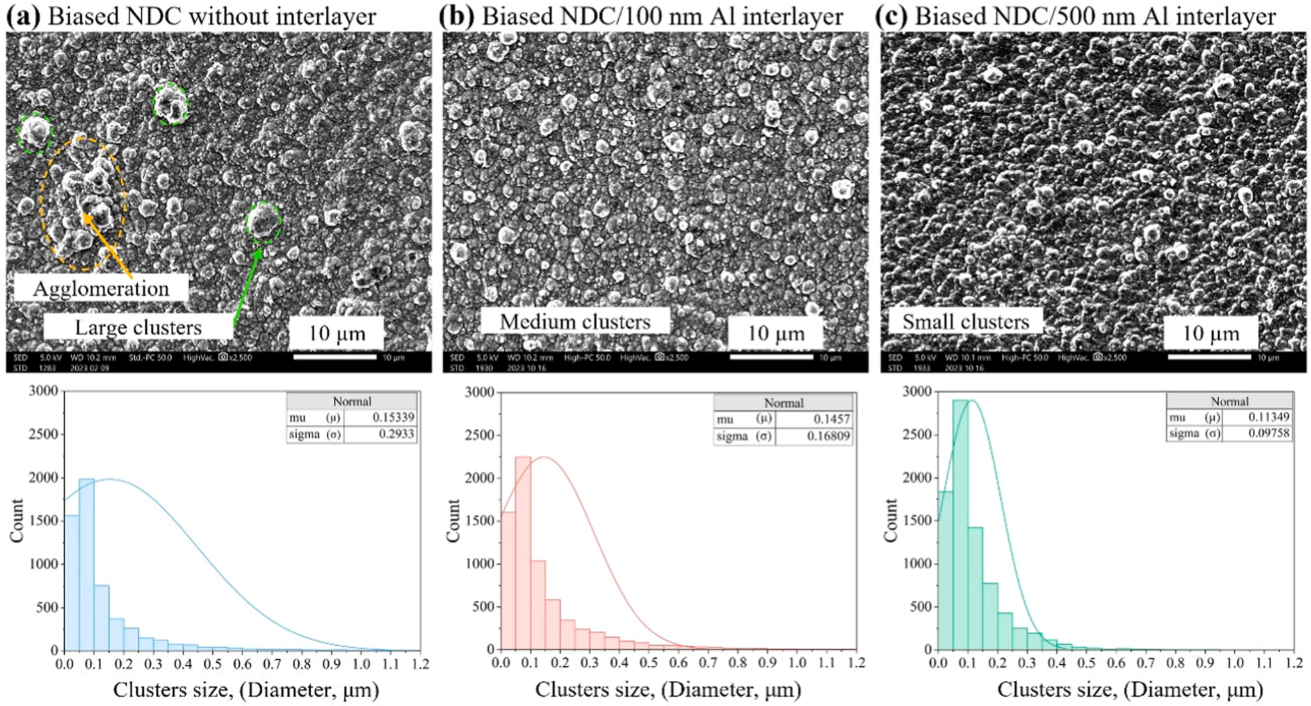
(a) Biased NDC without interlayer
(b) Biased NDC/100 nm Al interlayer
(c) Biased NDC/500 nm Al interlayer

Fig. 3. (Colour online) Top-view FE-SEM images with associated image-J analysis of biased NDC films deposited without, with 100 nm, and with 500 nm Al interlayer.

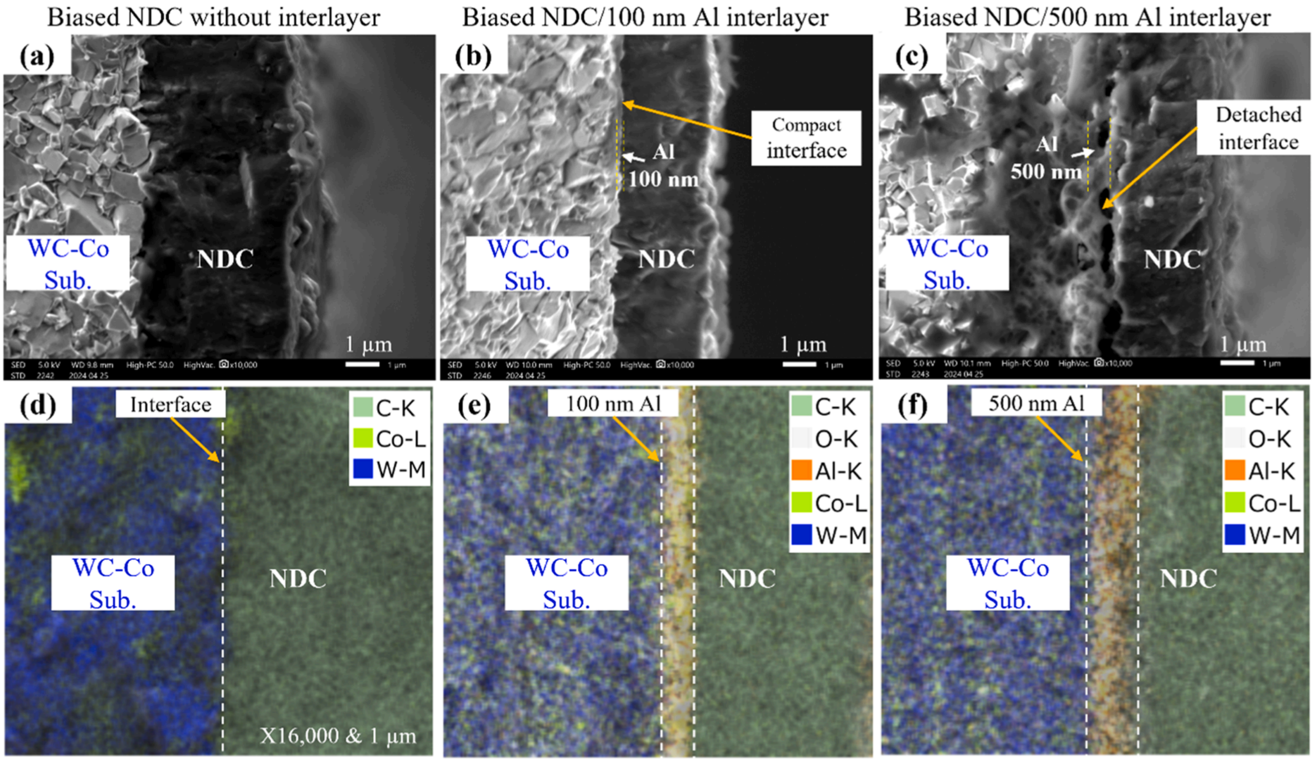

Fig. 4. (Colour online) Cross-sectional FE-SEM images and EDS mapping of biased NDC coatings fabricated: (a, d) directly without interlayer, (b,e) with 100 nm Al interlayer, and (c,f) with 500 nm Al interlayer on WC−Co substartes.

substrate exhibits a homogeneous structure with clustering patterns resembling formations of cauliflower-like clusters. Cluster sizes were analysed using the free ImageJ software [42]. Initially, films without an interlayer (Fig. 3a) exhibited an average cluster size (µ) of ≤153 nm. The introduction of an Al interlayer reduced surface roughness, which in turn correlated with a decrease in cluster growth and aggregation. Consequently, films with an Al interlayer displayed smaller and more uniformly distributed clusters, with an average size of ≤113 nm (Fig. 3c). Furthermore, as the Al interlayer thickness increased from 0 nm to 500 nm, the overall cluster count (Y-axis) increased gradually, while both the average cluster size and the dispersion (σ) decreased steadily, with σ values falling from 293 to 168 and finally to 98 nm.

Furthermore, the application of a negative substrate bias (−100 V) during deposition resulted in a notable reduction in the clusters size and a more compact film structure compared to un-biased depositions reported in our previous work [34]. This observation is attributed to the transfer of increased energy to surface adatoms during biased deposition. This enhanced energy is hypothesized to improve the mobility of surface adatoms [43,44]. This improved mobility likely contributes to a denser film structure by promoting grain refinement through several mechanisms: filling voids between existing grains, disrupting large columnar grain growth, and creating additional nucleation sites.

The interplay between the highly energitic carbon species emitted from the CAPD-anode and the roughened WC−Co substrate surface (Ra = 100 ± 10 nm) significantly influenced the film growth. This combination facilitated the achievement of a dense film with a thickness of approximately 3 µm ± 0.5 µm and an impressive deposition rate ranging from 2.1 to 3.3 µm/hour.

The impact of Al interlayer thickness on the film-substrate interface was systematically investigated. Cross-sectional FE-SEM images (Fig. 4c) revealed partial detachment at the interface for samples with a thicker Al interlayer (500 nm), whereas samples with a thinner Al interlayer (100 nm) exhibited a more compact and uniform film structure, with no visible signs of delamination. EDS mapping (Fig. 4d–f) further confirmed variations in Al interlayer thickness, showing a more intense Al signal in the thicker interlayer (500 nm) compared to the thinner one (100 nm), as evidenced by the pronounced orange coloration. This variation also suggests differences in oxidation levels associated with interlayer thickness. These findings highlight the critical role of optimizing Al interlayer thickness to improve adhesion between the NDC film and the WC–Co substrate.

Three-dimensional laser microscopy was employed to quantify the surface roughness of the deposited NDC films, as shown in Fig. 5. The arithmetic average roughness (Ra) and the arithmetical mean height (Sa) were evaluated for biased NDC coatings with and without the Al interlayer. These roughness parameters were compared to those of the bare WC−Co substrate and the Al interlayer itself (Fig. 6).

The surface morphology of the NDC coatings exhibited a characteristic "cauliflower-like" structure composed of individual particles and their boundaries (Figs. 3a and 5c). This morphology is attributed to the limited mobility of initially adsorbed atoms on the substrate due to insufficient energy from the incident particles to overcome surface diffusion barriers [44,45]. Consequently, these atoms adhere directly to the substrate, forming the observed clustered features. Interestingly, the application of a negative substrate bias (−100 V) during deposition resulted in the formation of numerous hillocks on the film surface, creating a quasi-columnar topography (Fig. 5c).

The Al interlayer's presence and thickness had a substantial influence on the NDC films' final surface roughness. The roughness value remained stable as the Al interlayer thickness increased, yet it was consistently lower than the bare WC—Co substrate (Fig. 5a-b). Remarkably, the biased NDC coatings fabricated on the Al interlayer displayed a dense and ultra-smooth surface morphology devoid of hillocks (Fig. 5d-e). This observation aligns well with the featureless surface morphologies observed in the corresponding FE-SEM images (Fig. 3a-c).

Roughness parameters, including Ra and Sa, showed an increase in films deposited without an interlayer (Fig. 6). This increase may be linked to the enlargement of sp^2 carbon clusters, which could have been promoted by the negative bias voltage attracting a larger proportion of non-sp^3 carbon phases to the surface, contributing to the rise in surface

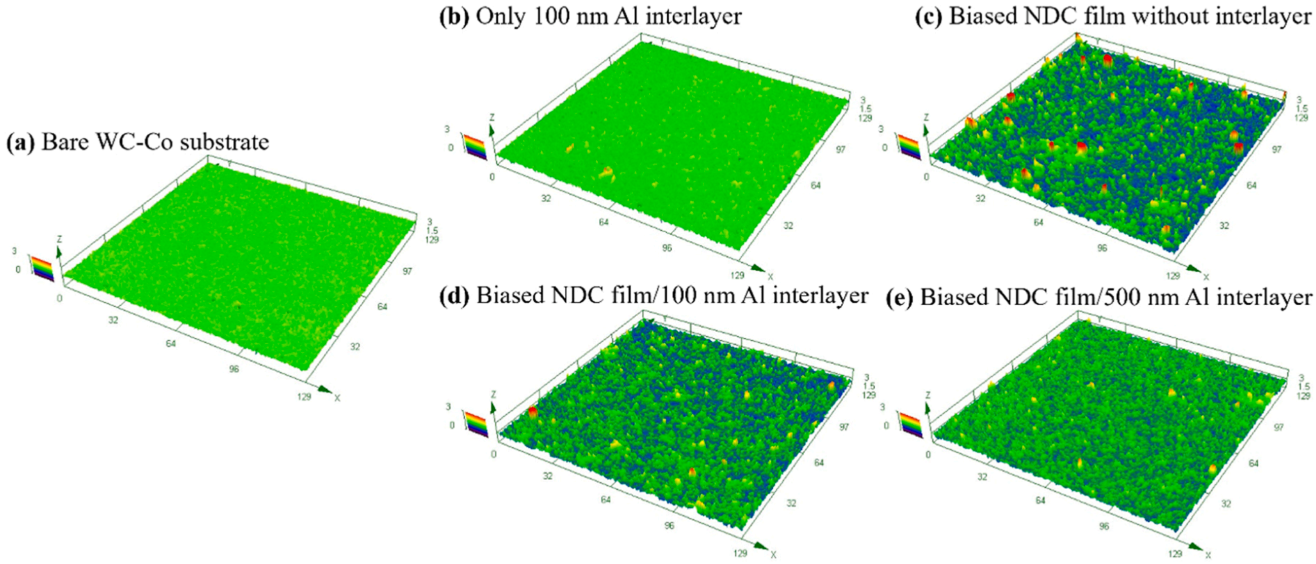

Fig. 5. (Colour online) Surface topography using 3D laser microscopy for: (a) bare WC−Co substrate, (b) 100 nm Al interlayer, and biased NDC films deposited on WC−Co substrates: (c) without Al interlayer, (d) with 100 nm Al interlayer, and (e) with 500 nm Al interlayer.

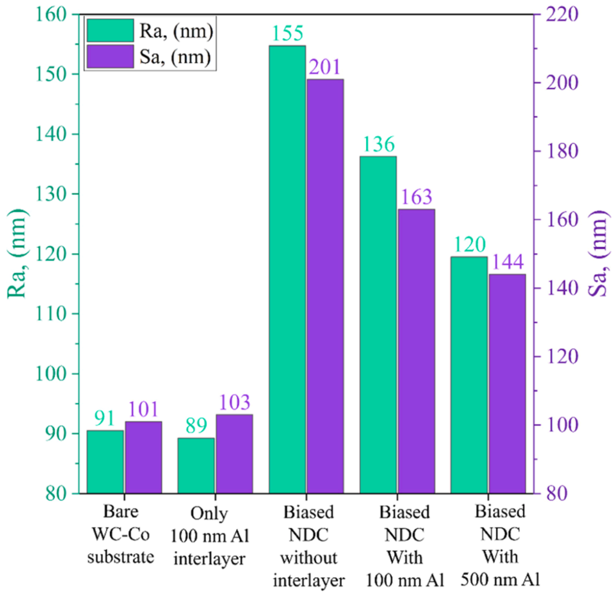

Fig. 6. (Colour online) Summery of surface roughness (Ra and Sa) of investigated NDC films compared to bare WC−Co substrate and 100 nm Al interlayer.

roughness [37]. This trend is evident from the increase in Ra values, which rose from 91 nm to 155 nm for biased films without an interlayer.

The Al interlayer, however, played a significant role in mitigating the increase in roughness. Introduction of the Al interlayer reduced Ra from 155 nm to 136 nm, and further reduction occurred as the interlayer thickness increased from 100 nm to 500 nm, with Ra decreasing from 136 nm to 120 nm. This improvement is likely due to the bombardment of higher energetic particles on the surface bulges, effectively etching their tops and filling adjacent valleys, resulting in a smoother surface and enhanced attraction of non-sp^3 carbon phases.

Notably, the surface roughness of the films deposited with the Al interlayer closely resembled the initial roughness of the substrate and Al interlayer itself, approximately 90 nm. This finding indicates that the Al interlayer has a pivotal role in determining the final surface roughness of the NDC films.

3.3. Raman spectra analysis

Raman spectroscopy is a powerful tool for characterizing carbon-based films due to its ability to differentiate between sp^2 and sp^3 hybridized carbon atoms, as well as estimate the domain size of these phases within the film [46]. Fig. 7 displays the Raman spectra of NDC coatings deposited on biased substrates both with and without Al interlayers. The recorded spectra exhibit characteristic bands similar to those observed in CVD diamond films [13], enabling a clear distinction between NDC films and hard diamond-like carbon (DLC) films. Notably, the presence of *trans*-polyacetylene (t-PA) peaks provides definitive evidence of grain boundaries, confirming the formation of diamond nanocrystallites in NDC films, comparable to those found in CVD diamond [47]. In contrast, such peaks are absent in DLC films due to their inherently amorphous structure.

The analysis of the Raman spectra reveals the coexistence of both nanodiamond crystals and graphitic phases on the surface of the NDC films. A typical NDC film spectrum consists of seven main peaks [32,48]: t-PA$_1$ (around 1170 cm^{-1}), diamond (around 1337 cm^{-1}), D (around 1345 cm^{-1}), t-PA$_2$ (around 1465 cm^{-1}), and the G-peak (cantered at approximately 1580 cm^{-1}, composed of G$_1$, G$_2$, and G$_3$ sub-peaks). The presence of shoulders on the t-PA$_1$ and t-PA$_2$ peaks indicates a significant number of grain boundaries within the film, likely a consequence of the nanodiamond phase formation. The G-peak originates from the stretching vibrations of sp^2 carbon atoms in chains or aromatic rings, whereas the d-peak stems from the breathing mode of sp^2 carbon atoms confined to aromatic rings.

Fig. 7a highlights the effect of substrate biasing on the nanostructure of the NDC coatings. A sharp and intense peak at approximately 1337 cm^{-1}, corresponding to the diamond phase, is observed. The application of substrate biasing leads to a significant enhancement in the intensity of this peak, indicating improved nanodiamond quality [34]. This enhancement can be attributed to the role of biasing in promoting the formation of C−C sp^3 bonds, which contributes to increased film hardness and wear resistance. However, the high intensity of the G-peak suggests that substrate biasing might also attract a larger proportion of non-sp^3 carbon phases to the surface, leading to a slight increase in the graphitic character. Additionally, the presence of non-etched Co on the substrate surface might contribute to surface graphitization.

Fig. 7b and c underscore the significant role of the Al interlayer in enhancing the growth and quality of nanodiamonds within the films deposited using the CAPD process. Similar to the observations with

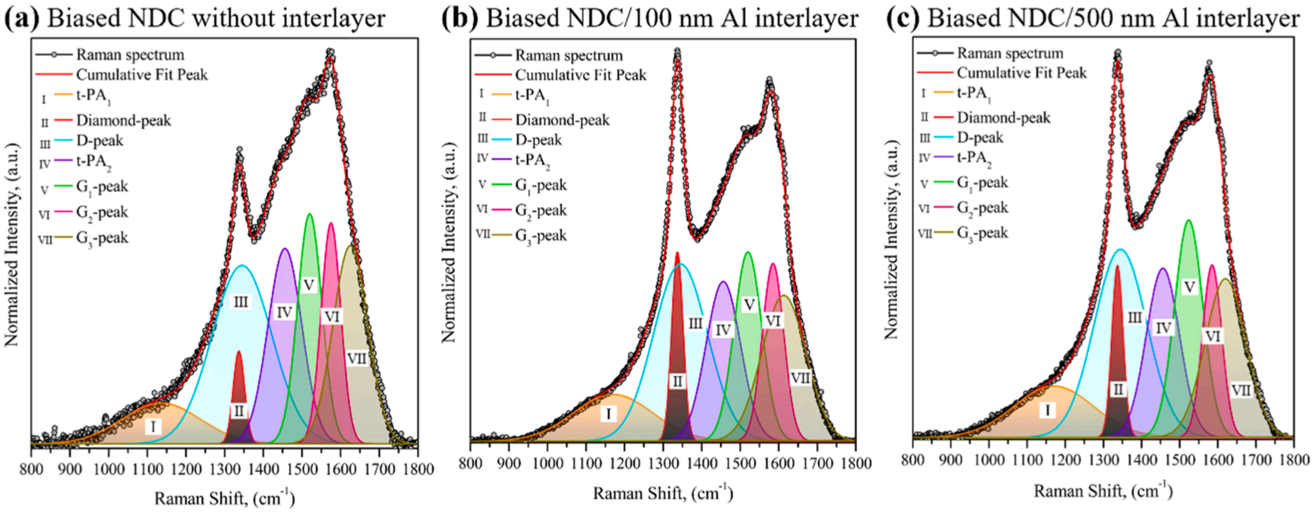

Fig. 7. (Colour online) Visible Raman spectra of NDC films deposited on biased WC−Co substrates with: (a) no interlayer, (b) 100 nm Al interlayer, and (c) 500 nm Al interlayer.

substrate biasing, an intense and sharp peak at around 1337 cm^{-1}, corresponding to the diamond phase, is observed. The peak intensity is further enhanced when substrate biasing is combined with an optimized Al interlayer thickness. These observations are in alignment with the findings derived from FE-SEM analysis and tribological testing.

3.4. Adhesion assesment

A critical challenging factor for NDC film performance is its adhesion strength to the substrate. Scratch testing, a reliable evaluation method, was used to assess this property. Fig. 8 combines the scratch test results (acoustic emission, normal force, and friction coefficient) with microscopic images of the scratch track for a more comprehensive analysis. A sharp increase in all three measured signals during the test signifies coating delamination. The critical load at which this delamination occurs serves as a quantitative measure of adhesion strength.

The results demonstrate a significant improvement in adhesion for biased NDC coatings deposited with a 100 nm Al interlayer (critical load = 17 N) in comparison with films without the interlayer (critical load = 9.5 N). Microscopic examination of the scratch track for the 100 nm interlayer case is expected to reveal good adhesion, supporting this finding. This highlights the beneficial role of the thin Al interlayer in completely hindering Co on the substrate surface and forming dense Al_2O_3, promoting stronger interfacial bonding between the film and the substrate.

However, increasing the Al interlayer thickness to 500 nm led to reductions in hardness, Young's modulus, and adhesion strength, with a critical load of 12.3 N. Microscopic analysis of the scratch track indicates possible delamination at the interface, consistent with the observed decline in adhesion strength. This behaviour is attributed to the formation of a thicker Al-rich interfacial layer (Fig. 3b) and elevated internal stress [49,50]. Given that aluminium is softer than the NDC film, the thicker layer introduced shear stress across the interlayer, further exacerbating internal stress and compromising adhesion. These findings highlight the adverse effects of excessive Al interlayer thickness on mechanical and tribological performance.

Complementing the scratch test results, Rockwell D toughness testing was conducted to further evaluate the Al interlayer's impact on adhesion strength. Fig. 9 reveals the stark difference in response to mechanical stress. The micrograph for the biased NDC film without the Al interlayer (Fig. 9a) shows extensive delamination around the indentation crater, signifying weak adhesion. This highlights the importance of adhesion strength in preventing film failure under mechanical stress.

Fortunately, the Al interlayer dramatically improves adhesion. As shown in Fig. 9b and c (100 nm and 500 nm Al interlayers, respectively), no apparent large cracks or spallation are observed around the craters. This remarkable improvement can be attributed to the Al interlayer potentially mitigating internal stresses within the film and suppressing the interfacial catalytic effects of cobalt. Cobalt can boost graphitization, weakening adhesion. By potentially suppressing this graphitization process, the Al interlayer indirectly strengthens the film-substrate bond.

The Rockwell D toughness test results strongly support the scratch test findings. They collectively demonstrate that the Al interlayer significantly enhances the adhesion strength of the NDC coating to the WC−Co substrate, a crucial factor for maintaining film integrity and performance under various mechanical stresses encountered in real-world applications.

The thickness of the Al interlayers significantly impacts the adhesion strength of NDC coatings fabricated on WC—Co substrates. A 100 nm thick Al interlayer significantly improves adhesion through two mechanisms. Firstly, it serves as a diffusion barrier, preventing Co migrating towards the film at the interface. This spatial separation isolates reactive C^+ species within the NDC film from direct contact with Co. Since Co promotes the formation of a weak, graphitic carbon layer at the interface, the Al interlayer effectively suppresses this detrimental graphitization process.

The Al interlayer undergoes oxidation, leading to the formation of a dense Al_2O_3 layer. This oxidation occurs both during the deposition process, due to residual oxygen in the sputtering chamber, and after deposition when the films are exposed to ambient air [51]. For instance, the residual atmosphere in the deposition chamber, with a base pressure of 5×10^{-3} Pa, predominantly contains nitrogen (N) and oxygen (O), with an approximate 20 % O, which facilitates the oxidation reaction. In the current experiment, the base pressure is 3×10^{-3} Pa, and the working pressure ranges from 0.5 to 0.5 Pa, contributing to the oxidation of the Al interlayer.

The resulting Al_2O_3 layer serves as a robust barrier, effectively restricting the diffusion of Co into the films and preventing its catalytic role in diamond graphitization at the interface. This is supported by the distinct oxygen (O) and aluminium (Al) signals observed in EDS mapping (Fig. 10). Additionally, XRD analysis reveals the formation of the Al_2O_3 phase, as referenced in JCPDS file no 71–1123 [52], confirming the presence of the oxide layer. This oxide layer plays a crucial role in hindering Co diffusion and enhancing adhesion, thereby improving the durability and performance of the coatings.

While a thin Al interlayer offers advantages, increasing its thickness to 500 nm has the opposite effect on adhesion strength. This is attributed to the formation of a thicker interfacial layer rich in aluminum. Aluminum itself has a lower inherent hardness compared to the NDC film. The presence of this thicker, softer layer weakens the overall mechanical properties of the film, including its adhesion to the substrate.

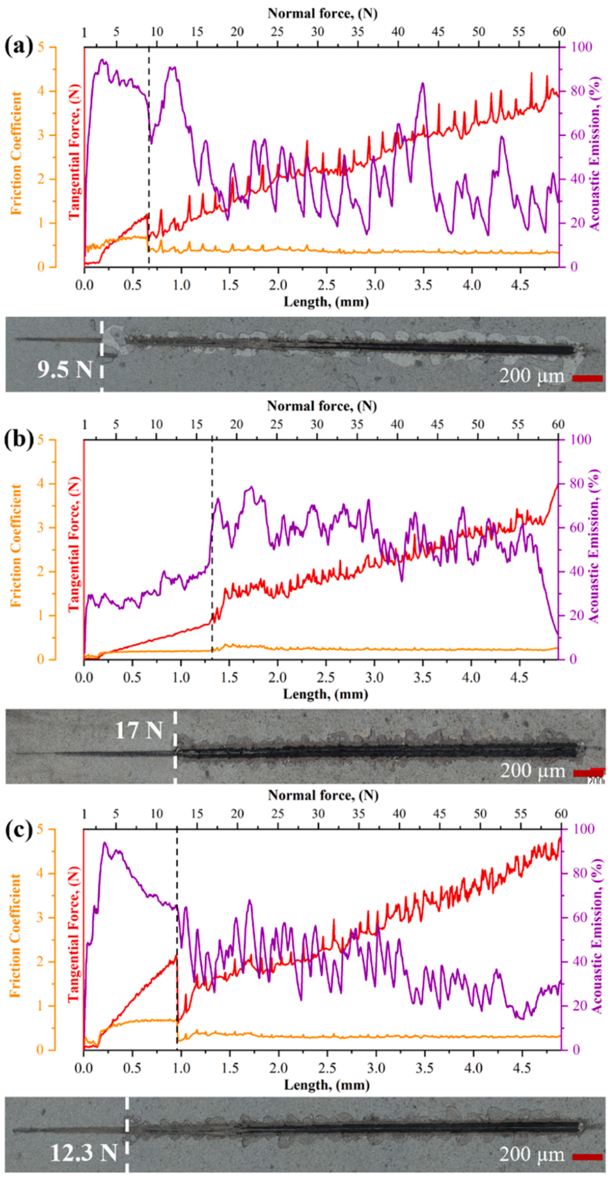

Fig. 8. (Colour online) Adhesion results of scratch test for NDC coatings deposited: (a) without interlayer, (b) with 100 nm Al interlayer, and (c) with 500 nm Al interlayer on biased WC−Co substrates.

The thickness of the Al interlayers remarkably influences the adhesion strength of NDC coatings deposited onto WC—Co substrates. A 100 nm Al layer enhances adhesion by inhibiting Co diffusion and graphitization through the formation of an Al oxide layer. Conversely, a thicker 500 nm layer weakens the film due to the presence of a softer Al-rich interface. Optimizing Al interlayer thickness is crucial for achieving strong adhesion. However, for cutting tool applications, the achieved maximum improvement in adhesion strength (critical load=17 N) is insufficient to meet the durability requirements for cutting tools applications.

3.5. *Tribological characteristics of NDC films*

NDC films demonstrate exceptional tribological performance under dry sliding conditions against Al_2O_3 counterparts, rendering them suitable for dry machining applications. Pin-on-disk tribometer tests (Fig. 11) show that biased NDC films without an Al interlayer exhibit a significantly lower coefficient of friction (COF $\approx$ 0.098) compared to the uncoated WC−Co substrate (COF = 0.31). This reduction in friction is accompanied by a lower wear rate for the NDC-coated samples (9.25×10^{-8} mm^3/N·m) in comparison with the uncoated substrate (2.07×10^{-7} mm^3/N·m), confirming the ability of NDC films to reduce friction and wear.

The introduction of a 100 nm Al interlayer before NDC deposition further enhances tribological performance by lowering the COF to 0.09 and stabilizing friction. This improvement is attributed to a smoother surface morphology and better wear resistance, as reflected in the wear rate of 7.85×10^{-8} mm^3/N·m, which is lower than both the reference NDC sample and the uncoated substrate. The Al interlayer serves to reduce surface asperities and provide a more stable interface during sliding.

The low coefficient of friction (COF) and wear rate of NDC films arise from several factors influencing tribological performance. In particular, the initially low surface roughness of the Al_2O_3 counterpart minimizes asperity contact and contributes to maintaining a stable COF. The smooth interfaces decrease mechanical interlocking between the contact surfaces, which is a primary cause of frictional losses during sliding. This effect is particularly notable in the initial stages of testing, where rougher surfaces with pronounced asperities typically lead to mechanical interlocking and fluctuations in COF, as observed in the friction tests between the rough Al_2O_3 counterpart (Ra = 355 nm, Sa = 427 nm) and the uncoated substrate (Fig. 11a). The initial contact pressure ($\approx$ 3 GPa), concentrated on asperities, causes fragmentation and the formation of third-body debris that rolls between the sliding surfaces, exacerbating

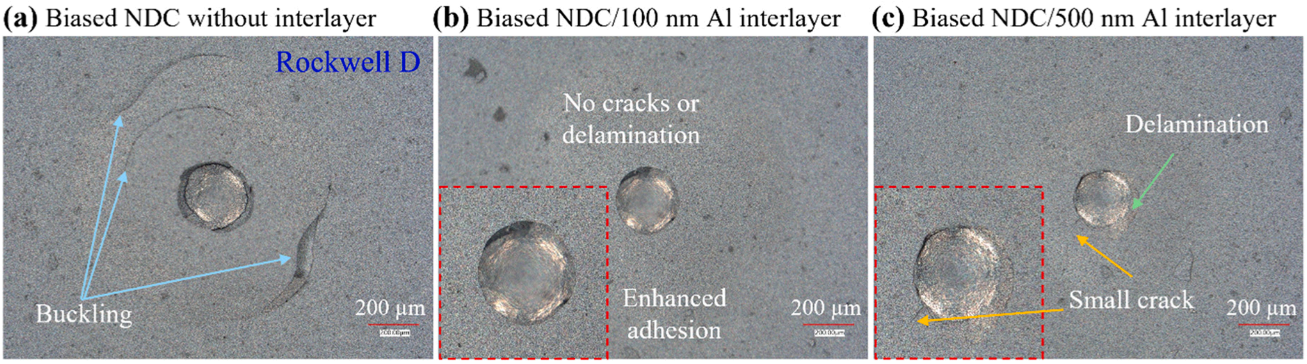

Fig. 9. (Colour online) Toughness mesurements using Rockwell D (100 Kgf) for NDC films deposited: (a) without interlayer, (b) with 100 nm Al interlayer, and (c) with 500 nm Al interlayer on biased WC−Co substrates.

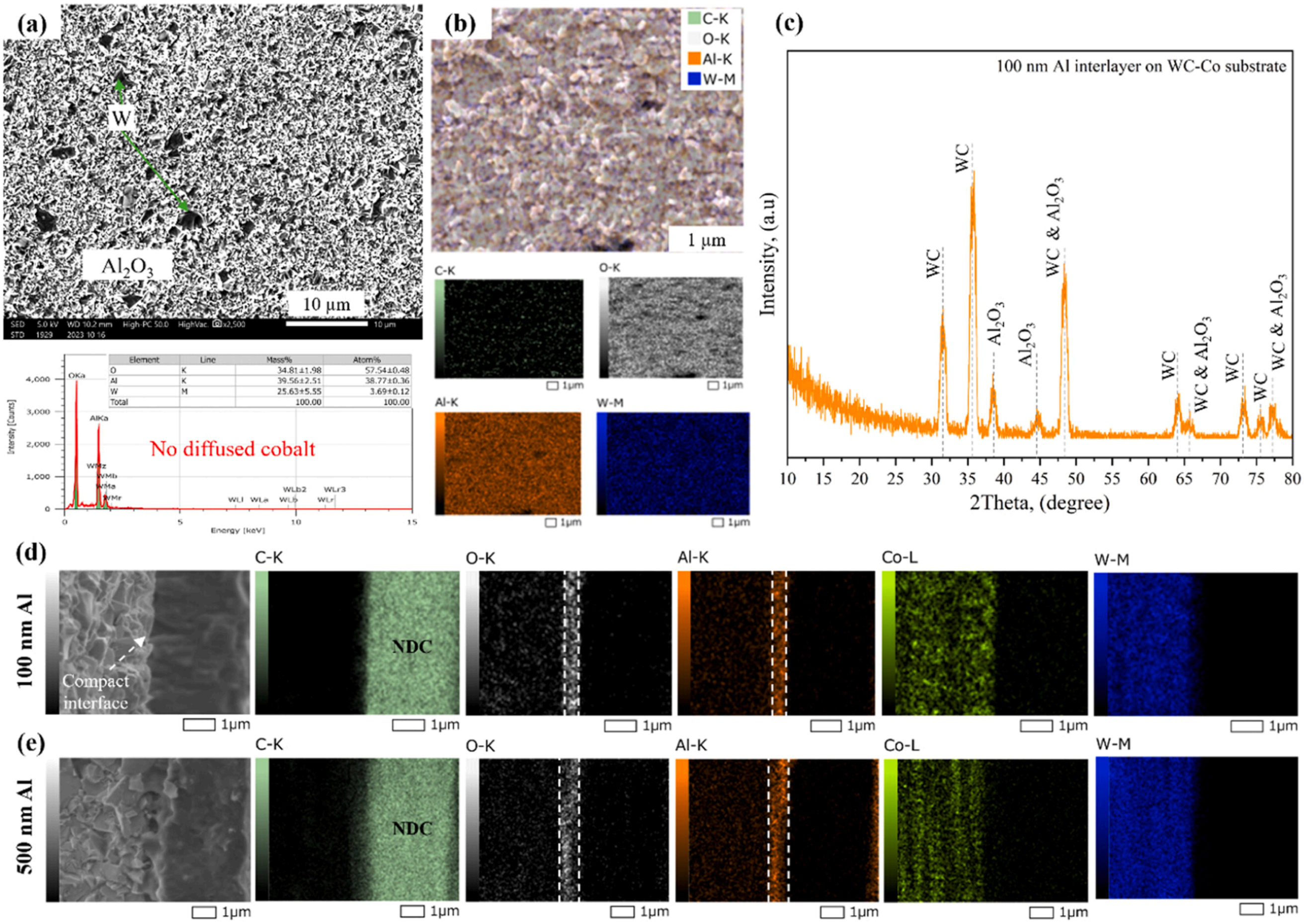

Element	Line	Mass%	Atom%
O	K	34.81±1.98	57.54±0.48
Al	K	39.56±2.51	38.77±0.36
W	M	25.63±5.55	3.69±0.12
Total		100.00	100.00

Fig. 10. (Colour online) (a) FE-SEM/EDS analysis of the WC−Co substrate with a 100 nm Al interlayer; (b) EDS surface mapping; (c) XRD analysis revealing the Al₂O₃ phase. Cross-sectional EDS mapping of NDC films with (d) 100 nm and (e) 500 nm Al interlayers, showing Al and O at the interface.

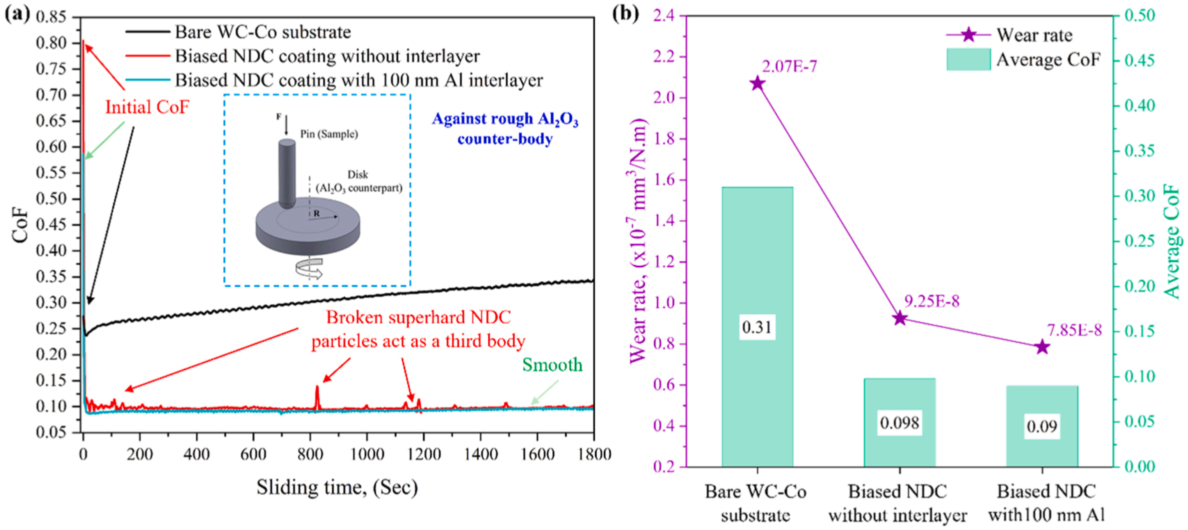

Fig. 11. (Colour online) Tribological properties of NDC film deposited without and with 100 nm aluminum interlayer vs. bare WC−Co substrate: (a) Friction curves, and (b) wear rate and average COF against alumina counter-body.

frictional instability.

However, when a smoother counterpart (Ra = 222.5 nm, Sa = 281 nm) is employed, the COF stabilizes more rapidly and decreases from 0.31 to 0.18 (Fig. 12). This smooth counterpart reduces asperity-induced fluctuations, facilitating a steadier tribological response. These findings suggest that surface roughness significantly influences friction and wear behaviour, as smoother surfaces minimize the mechanical interlocking and third-body abrasion associated with rougher counterparts.

Further analysis of NDC coatings without and with an Al interlayer reveals that the films with a 100 nm Al interlayer exhibit superior

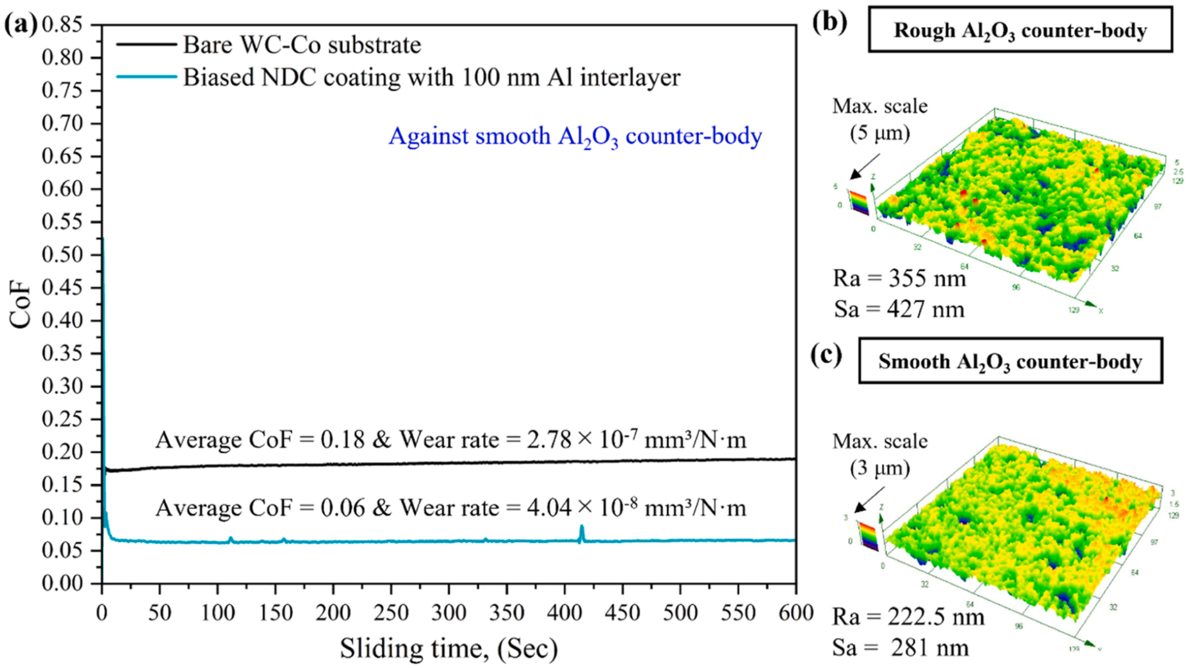

Fig. 12. (Colour online) (a) Friction curves comparing the tribological performance of an NDC film with 100 nm interlayer and an uncoated WC−Co substrate against a smooth Al_2O_3 counterpart, and 3D surface images of both (b) rough and (c) smooth Al_2O_3 counterparts.

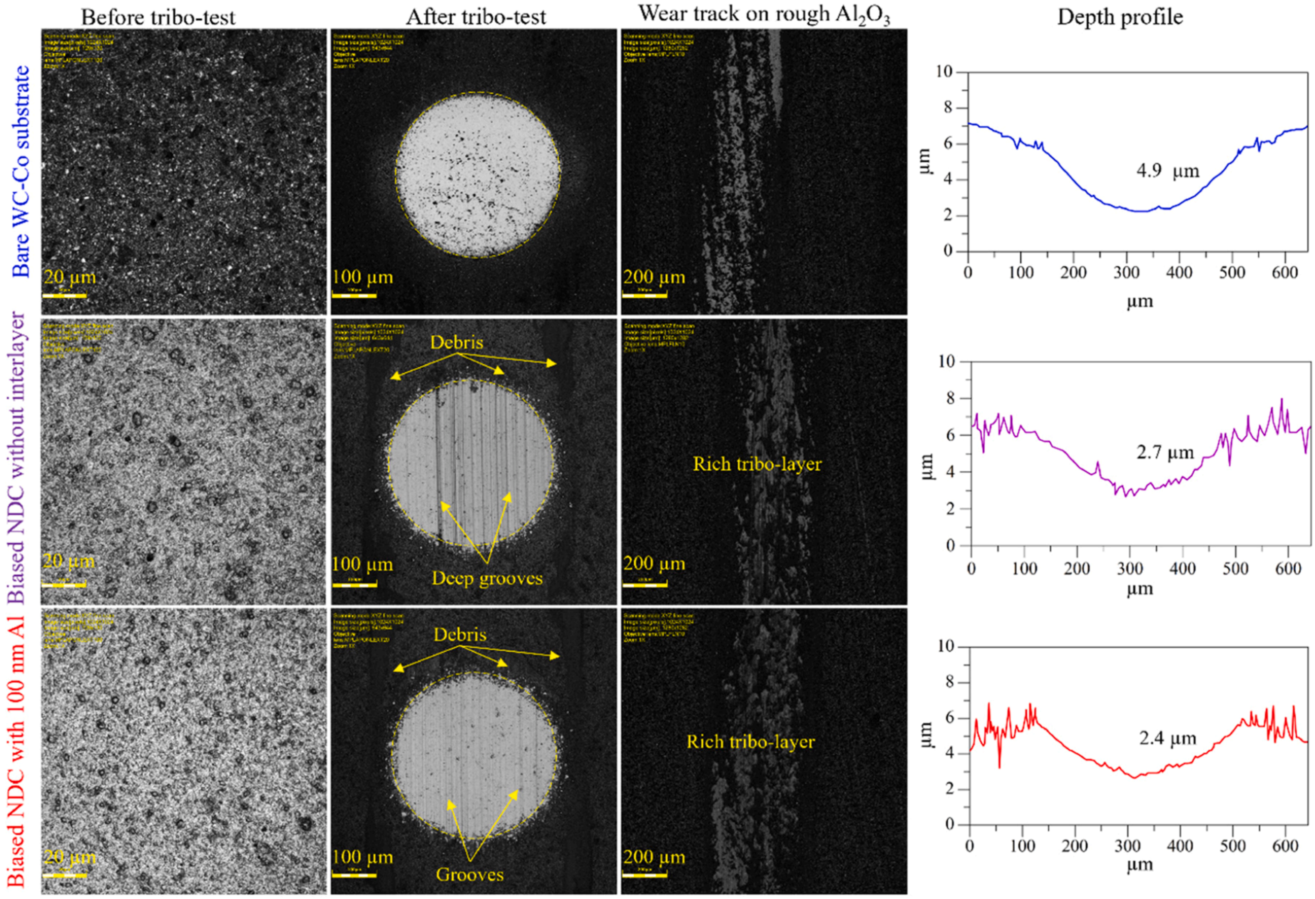

Fig. 13. (Colour online) Wear morphology of uncoated and NDC-coated WC−Co substrates with 0.0 and 100 nm Al interlayers, before and after friction testing, including roughened alumina wear tracks and depth profiles.

tribological performance. The initial COF of the biased NDC coatings with the Al interlayer was 0.56, which rapidly reached a steady state without fluctuations. In contrast, the reference NDC sample (without interlayer) exhibited a higher initial COF of 0.8, with more pronounced fluctuations before stabilizing. The smoother interface formed by the NDC film with Al interlayer is attributed to the higher toughness and hardness of the film, which allows broken asperities from the film surface to fill valleys on the opposing counterpart, resulting in a tribo-layer and stable COF. Conversely, the larger asperities from reference NDC films (without the interlayer) interlocked with the valleys of the counterpart surface, leading to deeper grooves and less stable friction behaviour.

The impact of counterpart roughness on friction and wear is further explored through additional experiments. NDC films with an Al interlayer showed a significantly lower COF (0.06) when tested against a smoother Al_2O_3 counterpart (Ra = 222.5 nm, Sa = 281 nm), compared to 0.09 when tested against a rougher counterpart (Ra = 355 nm, Sa = 427 nm). This demonstrates that fragmented asperities from rougher surfaces act as third-body particles, rolling at the interface and increasing both COF and wear rates. These results emphasize the critical role of initial asperities in determining the tribological performance of NDC films and their counterparts.

Surface analysis of the worn areas following tribological testing reveals furrows and debris, indicative of abrasive wear. This wear is attributed to the shearing and fracture of cauliflower-shaped particles on the NDC film surface, as well as the fragmentation of asperities on the rough Al_2O_3 counterpart (Fig. 13). A distinct tribo-layer is observed on the wear track of the counterpart. The measured wear depths correspond with the trends observed in the calculated wear rates based on the volume of debris. Specifically, NDC coatings with an Al interlayer exhibit the lowest wear depth (2.4 μm), compared to 2.7 μm for NDC films without the interlayer and 4.9 μm for the uncoated substrate.

Tribological analysis of the worn surfaces following friction testing against a rough counterpart (Fig. 12) reveals the mechanisms underlying wear. The NDC film surfaces show signs of abrasive wear, such as grooves and debris, resulting from the fracture of cauliflower-shaped particles under shear forces. This generates wear debris, which becomes trapped between the sliding surfaces, further exacerbating wear. However, as sliding progresses, the surfaces smoothen, and the COF stabilizes. The grain boundaries within the NDC films play a crucial role in this steady-state behaviour by facilitating surface smoothing and promoting the formation of a stable tribo-layer.

Fig. 14 illustrates a microscopic image and a closer inspection using a zoomed FE-SEM image, revealing a significant finding regarding the worn area of the NDC coating (with Al interlayer) after the tribological test against the rough Al_2O_3 counterpart. Apparent presence of debris particles originating from broken asperities in both the NDC film and the opposing ceramic material, as well as numerous grooves and wear marks indicate that abrasive wear is the dominant mechanism. However, due to the inherently smooth surface structure and superior mechanical properties of the NDC films, the wear marks appear smooth and shallow, with minimal signs of peeling or large-scale material removal. This observation highlights the film's ability to withstand severe wear conditions.

The extraordinary tribological behaviour of NDC films is attributed, in part, to the genesis of a stable and protective tribo-film during dry sliding. This tribo-layer's formation is driven by two key factors: the abundant grain boundaries within the NDC film and the high contact pressure experienced during testing [53]. These features facilitate the rehybridization of carbon atoms from their original diamond-like (sp^3) bonding to a more lubricating graphite-like (sp^2) structure [30]. This transformation is crucial, as the newly formed tribo-film performs as a solid lubricant, notably decreasing friction and wear.

Raman spectroscopy, shown in Fig. 14c, provides insights into this phenomenon. During the tribological test, the carbon atoms within the NDC film undergo a structural rearrangement, transforming into a more lubricating graphite-like form [54]. This transformation is evident from the augmented intensity of the G-band in comparison with the d-band and diamond band in the Raman spectra, in contrast to the as-deposited film (Fig. 7). This graphitization process likely contributes to the creation of a lubricating layer at the contact area between the NDC film and the Al_2O_3 counterpart, further reducing friction [55].

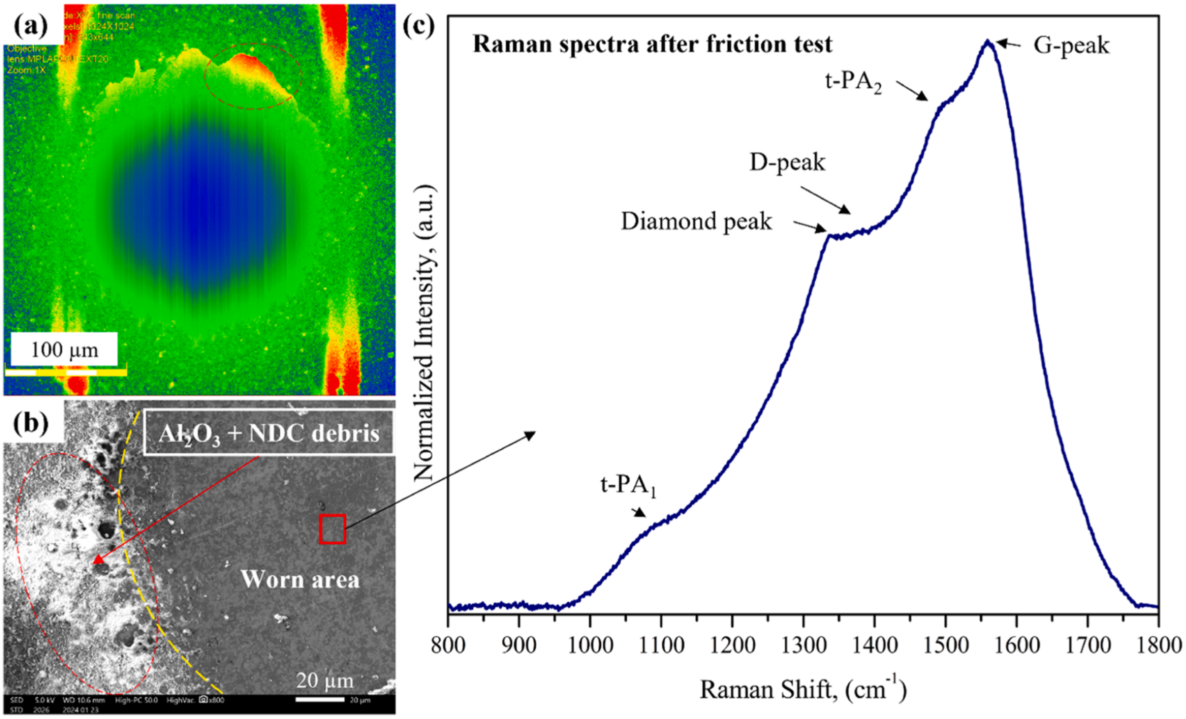

Fig. 14. (Colour online) Post-friction test analysis to elucidate tribo-film formation after 30 min of sliding against Al_2O_3 counter body: (a) Wear morphology, (b) FE-SEM image, and (c) Raman spectra of NDC coatings deposited with 100 nm Al interlayer on pin-shaped WC−Co substrate.

The formation of this protective tribo-layer, driven by film graphitization under high contact pressure and facilitated by grain boundaries, is a critical factor in the superior tribological performance of NDC films. This tribo-layer functions as a solid lubricant, decreasing both friction coefficient and wear rate. NDC films, with their high hardness (75 GPa), toughness, and self-lubricating properties, exhibit exceptional anti-wear resistance, making them suitable for dry machining applications. The films meet the requirements for such applications, demonstrating a low friction coefficient (COF ≤ 0.1) and a high wear resistance (wear rate $\leq$ 10ˆ−6 mm^3/N·m). These tribological characteristics result in reduced heat generation, minimized tool wear, and improved workpiece integrity, thus leading to cost-effective machining operations with prolonged tool life and enhanced dimensional precision.

4. Conclusion

NDC coatings were deposited on biased WC−Co substrates using coaxial arc plasma deposition, resulting in film hardness of 70.8 GPa. However, the use of $a - 100$ V bias voltage compromised adhesion strength due to the catalytic effect of cobalt (Co), which promotes graphitization and weakens adhesion by transforming sp^3 carbon bonds into weaker sp^2 bonds. To address this issue, the study explored the incorporation of aluminum (Al) interlayers with thicknesses of 0, 50, 100, 300, and 500 nm, deposited via DC sputtering before NDC deposition. The experiemens investigated that a 100 nm Al interlayer effectively mitigates Co-induced graphitization by forming a dense Al_2O_3 layer at the interface. This configuration serves as an optimal diffusion barrier, enhancing both adhesion strength and tribological characteristics of the NDC coatings. The NDC films with a 100 nm Al interlayer demonstrated a 79 % increase in adhesion strength, as evidenced by a 17 N critical load for full spallation during scratch testing. Furthermore, these films exhibited a 62 % improvement in wear resistance, with a wear rate of 7.85×10^{-8} mm^3/N.m, and a significantly lower coefficient of friction (COF ≤ 0.09) during dry sliding against an Al_2O_3 counterpart, representing a 71 % reduction compared to the bare substrate. These enhancements are attributed to the refined nanostructure of the NDC films, characterized by a rich grain-boundary network, along with superior mechanical features (hardness of 75 GPa and Young's modulus of 724 GPa) resulting from the combination of substrate biasing and the optimized Al interlayer. The findings provide valuable insights into improving durability and coating performance, presenting a promising solution for extending tool lifetime and enhancing efficiency in dry friction applications. However, further enhancement of the film-substrate adhesion strength is necessary to meet the durability requirements for dry machining.

Author statement

This study introduces a novel approach by optimizing the thickness of an aluminum (Al) interlayer (0.0, 50, 100, 300, and 500 nm) in conjunction with the application of a biasing voltage (−100 V). The Al interlayer effectively suppresses the diffusion and catalytic effects of the Co element on WC−6 %Co substrates, while the biasing voltage enhances plasma ionization, improving the hardness and wear resistance of nanodiamond composite (NDC) coatings. Unlike prior studies, which focused on individual factors, this work systematically explores the durability, friction, and wear performance of NDC films by combining Al interlayer optimization with biasing voltage. The 100 nm Al interlayer forms a protective Al_2O_3 layer, leading to a 79 % increase in adhesion strength, a 62 % improvement in wear resistance, and a 71 % reduction in friction. These findings provide deeper insights into the mechanisms of enhanced tribological performance, offering a promising solution for cutting tools in dry machining conditions. However, the durability improvements are still limited by low adhesion strength (Critical load of 17 N), which remains a critical factor for cutting tools in such environments.

CRediT authorship contribution statement

Mohamed Ragab Diab: Writing – original draft, Validation, Methodology, Formal analysis. **Koki Murasawa:** Resources, Methodology. **Mei Wang:** Validation, Methodology. **Shinya Ohmagari:** Validation, Methodology. **Hiroshi Naragino:** Methodology, Investigation. **Tsuyoshi Yoshitake:** Writing – review & editing, Supervision, Funding acquisition. **Mohamed Egiza:** Writing – review & editing, Writing – original draft, Conceptualization, Project administration.

Declaration of competing interest

The authors declare that they have no known competing financial interests or personal relationships that could have appeared to influence the work reported in this paper.

Acknowledgements

The first author, Mohamed Diab, a Ph.D. student at Kyushu University, thanks his research team and anonymous reviewers for their support and contributions. This research received partial financial support from Osawa Scientific Studies Grants Foundation, Advanced Machining Technology & Development Association, JST A-STEP Stage II (Grant Number S2915051S) and JSAP KEKENHI (Grant Number JP19H02436).

Data availability

Data will be made available on request.

References

[1] A. Inspektor, P.A. Salvador, Architecture of PVD coatings for metalcutting applications: a review, Surf. Coat. Technol. 257 (2014) 138–153, https://doi.org/10.1016/j.surfcoat.2014.08.068.

[2] L. Ortiz-Membrado, S. García-González, J. Orrit-Prat, R. Bonet, J. Caro, J.F. de Ara, E. Almandoz, L. Llanes, E. Jiménez-Piqué, Improved adhesion of cathodic arc PVD AlCrSiN coating on ion-implanted WC-Co substrates, Int. J. Refract. Metal. Hard Mater. 113 (2023) 106187, https://doi.org/10.1016/j.ijrmhm.2023.106187.

[3] A. Bicherl, T. Zimmerl, G. Mühlbauer, S. Geroldinger, A. Bock, When tungsten meets carbon, Int. J. Refract. Metal. Hard Mater. 119 (2024) 106448, https://doi.org/10.1016/j.ijrmhm.2023.106448.

[4] T. Kagnaya, C. Boher, L. Lambert, M. Lazard, T. Cutard, Microstructural analysis of wear micromechanisms of WC–6Co cutting tools during high speed dry machining, Int. J. Refract. Metal. Hard Mater. 42 (2014) 151–162, https://doi.org/10.1016/j.ijrmhm.2013.08.017.

[5] G.S. Goindi, P. Sarkar, Dry machining: a step towards sustainable machining –challenges and future directions, J. Clean. Prod. 165 (2017) 1557–1571, https://doi.org/10.1016/j.jclepro.2017.07.235.

[6] K. Weinert, I. Inasaki, J.W. Sutherland, T. Wakabayashi, Dry machining and minimum quantity lubrication, CIRP Annals 53 (2) (2004) 511–537, https://doi.org/10.1016/S0007-8506(07)60027-4.

[7] P.S. Sreejith, B.K.A. Ngoi, Dry machining: machining of the future, J. Mater. Process. Technol. 101 (1) (2000) 287–291, https://doi.org/10.1016/S0924-0136(00)00445-3.

[8] T. Bakša, T. Kroupa, P. Hanzl, M. Zetek, Durability of cutting tools during machining of very hard and solid materials, Procedia Eng. 100 (2015) 1414–1423, https://doi.org/10.1016/j.proeng.2015.01.511.

[9] R. Polini, M. Barletta, G. Rubino, S. Vesco, Recent advances in the deposition of diamond coatings on Co-cemented tungsten carbides, Adv. Mater. Sci. Eng. 2012 (1) (2012) 151629, https://doi.org/10.1155/2012/151629.

[10] X. Liu, H. Zhang, G. Lin, Z. Wang, J. Zhang, H. Shi, Advances in deposition of diamond films on cemented carbide and progress of diamond coated cutting tools, Vacuum. 217 (2023) 112562, https://doi.org/10.1016/j.vacuum.2023.112562.

[11] J. Zhang, X. Wang, B. Shen, F. Sun, Effect of boron and silicon doping on improving the cutting performance of CVD diamond coated cutting tools in machining CFRP, Int. J. Refract. Metal. Hard Mater. 41 (2013) 285–292, https://doi.org/10.1016/j.ijrmhm.2013.04.017.

[12] L. Wang, X. Lei, B. Shen, F. Sun, Z. Zhang, Tribological properties and cutting performance of boron and silicon doped diamond films on Co-cemented tungsten carbide inserts, Diam. Relat. Mater. 33 (2013) 54–62, https://doi.org/10.1016/j.diamond.2013.01.004.

[13] K. Murasawa, M.R. Diab, H. Atta, H. Naragino, A. El-Shaer, T. Yoshitake, M. Egiza, Disclosing mechanical and specific structural characteristics of thick and adherent nanodiamond composite hard coating deposited on WC−Co substrates, Mater. Today Commun. 40 (2024), https://doi.org/10.1016/j.mtcomm.2024.109839.

[14] D.-d. Ma, Y.-p. Xue, J. Gao, Y. Ma, S.-w. Yu, Y.-s. Wang, C. Xue, H.-j. Hei, B. Tang, Effect of Ta diffusion layer on the adhesion properties of diamond coating on WC-Co substrate, Appl. Surf. Sci. 527 (2020) 146727, https://doi.org/10.1016/j.apsusc.2020.146727.

[15] X. Lei, B. Shen, L. Cheng, F. Sun, M. Chen, Influence of pretreatment and deposition parameters on the properties and cutting performance of NCD coated PCB micro drills, Int. J. Refract. Metal. Hard Mater. 43 (2014) 30–41, https://doi.org/10.1016/j.ijrmhm.2013.10.016.

[16] F. Xu, J.H. Xu, M.F. Yuen, L. Zheng, W.Z. Lu, D.W. Zuo, Adhesion improvement of diamond coatings on cemented carbide with high cobalt content using PVD interlayer, Diam. Relat. Mater. 34 (2013) 70–75, https://doi.org/10.1016/j.diamond.2013.01.012.

[17] M.R. Diab, M. Egiza, K. Murasawa, S. Ohmagari, H. Naragino, T. Yoshitake, Revealing mechanical and structural properties of Si-doped nanodiamond composite films through applied biasing voltages on WC − Co substrates, Int. J. Refract. Metal. Hard Mater. 119 (2024), https://doi.org/10.1016/j.ijrmhm.2023.106518.

[18] R. Polini, F.P. Mantini, M. Braic, M. Amar, W. Ahmed, H. Taylor, Effects of Ti- and Zr-based interlayer coatings on the hot filament chemical vapour deposition of diamond on high speed steel, Thin. Solid. Films. 494 (1) (2006) 116–122, https://doi.org/10.1016/j.tsf.2005.08.219.

[19] K.K. Gajrani, S. Suresh, M.R. Sankar, Environmental friendly hard machining performance of uncoated and MoS2 coated mechanical micro-textured tungsten carbide cutting tools, Tribol. Int. 125 (2018) 141–155, https://doi.org/10.1016/j.triboint.2018.04.031.

[20] P. Lu, H. Gomez, X. Xiao, M. Lukitsch, D. Durham, A. Sachdeve, A. Kumar, K. Chou, Coating thickness and interlayer effects on CVD-diamond film adhesion to cobalt-cemented tungsten carbides, Surf. Coat. Technol. 215 (2013) 272–279, https://doi.org/10.1016/j.surfcoat.2012.08.093.

[21] O. Glozman, A. Berner, D. Shechtman, A. Hoffman, Influence of Cr-N interlayer properties on the initial stages of CVD diamond growth on steel substrates, Diam. Relat. Mater. 7 (2–5) (1998) 597–602, https://doi.org/10.1016/S0925-9635(97)00176-3.

[22] Y.S. Li, A. Hirose, Diamond growth on Fe-Cr-Al alloy by H2-plasma enhanced graphite etching, J. Appl. Phys. 101 (7) (2007), https://doi.org/10.1063/1.2717013.

[23] Y.S. Li, A. Hirose, The effects of substrate compositions on adhesion of diamond films deposited on Fe-base alloys, Surf. Coat. Technol. 202 (2) (2007) 280–287, https://doi.org/10.1016/j.surfcoat.2007.05.037.

[24] M. Egiza, M. Ragab Diab, A.M. Ali, K. Murasawa, T. Yoshitake, Sustainable super-hard and thick nanodiamond composite film deposited on cemented carbide substrates with an interfacial Al-interlayer, Mater. Lett. 364 (2024), https://doi.org/10.1016/j.matlet.2024.136369.

[25] Y. Tang, Y.S. Li, Q. Yang, A. Hirose, Deposition and characterization of diamond coatings on WC-Co cutting tools with W/Al interlayer, Diam. Relat. Mater. 19 ((5) (2010) 496–499, https://doi.org/10.1016/j.diamond.2009.12.019.

[26] Y.S. Li, Y. Tang, Q. Yang, C. Xiao, A. Hirose, Diamond deposition on steel substrates with an Al interlayer, Int. J. Refract. Metal. Hard Mater. 27 (2) (2009) 417–420, https://doi.org/10.1016/j.ijrmhm.2008.09.015.

[27] F. Ye, Y. Li, X. Sun, Q. Yang, C.-Y. Kim, A.G. Odeshi, CVD diamond coating on WC-Co substrate with Al-based interlayer, Surf. Coat. Technol. 308 (2016) 121–127, https://doi.org/10.1016/j.surfcoat.2016.06.088.

[28] Y.S. Li, Y. Tang, Q. Yang, S. Shimada, R. Wei, K.Y. Lee, A. Hirose, Al-enhanced nucleation and adhesion of diamond films on WC–Co substrates, Int. J. Refract. Metal. Hard Mater. 26 (5) (2008) 465–471, https://doi.org/10.1016/j.ijrmhm.2007.11.001.

[29] M.R. Diab, M. Egiza, K. Murasawa, H. Naragino, A. El-Shaer, T. Yoshitake, Eco-friendly thick and wear-resistant nanodiamond composite hard coatings deposited on WC–Co substrates, Surf. Coat. Technol. 479 (2024), https://doi.org/10.1016/j.surfcoat.2024.130517.

[30] M. Egiza, M.R. Diab, A.W. Zia, K. Murasawa, N. Faisal, T. Yoshitake, Wear-resistant and adherent nanodiamond composite thin film for durable and sustainable silicon carbide mechanical seals, Wear. 550 (551) (2024) 205394, https://doi.org/10.1016/j.wear.2024.205394.

[31] M. Egiza, A.M. Ali, K. Murasawa, T. Yoshitake, B-doped nanodiamond composite hard coatings deposited on cemented carbide: mechanical, structural, and tribological properties, Int. J. Refract. Metal. Hard Mater. 114 (2023), https://doi.org/10.1016/j.ijrmhm.2023.106260.

[32] M. Egiza, M.R. Diab, K. Murasawa, H. Naragino, T. Yoshitake, Nanomechanical and structural characteristics of nanodiamond composite films dependent on target-substrate distance, Arab. J. Sci. Eng. (2024), https://doi.org/10.1007/s13369-024-09161-9.

[33] M. Egiza, A.M. Ali, M.R. Diab, N. Hemaya, K. Murasawa, T. Yoshitake, Synthesis and comprehensive synchrotron-based structural analysis of Si-doped nanodiamond composite films deposited on cemented carbide, Surf. Coat. Technol. 471 (2023), https://doi.org/10.1016/j.surfcoat.2023.129867.

[34] M. Egiza, M.R. Diab, A.M. Ali, K. Murasawa, T. Yoshitake, Clean and durable thick nanodiamond composite hard coating deposited on cemented carbide towards sustainable machining: eco-friendly fabrication, characterization, and 3-E analysis, Clean. Eng. Technol. 22 (2024), https://doi.org/10.1016/j.clet.2024.100804.

[35] A.M. Ali, M. Egiza, K. Murasawa, Y. Fukui, H. Gonda, M. Sakurai, T. Yoshitake, Negative bias effects on deposition and mechanical properties of ultrananocrystalline diamond/amorphous carbon composite films deposited on cemented carbide substrates by coaxial arc plasma, Diam. Relat. Mater. 96 (2019) 67–73, https://doi.org/10.1016/j.diamond.2019.04.031.

[36] M.R. Diab, M. Egiza, K. Murasawa, H. Naragino, A. El-Shaer, T. Yoshitake, Eco-friendly thick and wear-resistant nanodiamond composite hard coatings deposited on WC–Co substrates, Surf. Coat. Technol. 479 (2024) 130517, https://doi.org/10.1016/j.surfcoat.2024.130517.

[37] M.R. Diab, M. Egiza, K. Murasawa, S. Ohmagari, H. Naragino, T. Yoshitake, Revealing mechanical and structural properties of Si-doped nanodiamond composite films through applied biasing voltages on WC − Co substrates, Int. J. Refract. Metal. Hard Mater. 119 (2024) 106518, https://doi.org/10.1016/j.ijrmhm.2023.106518.

[38] G.G. Adams, M. Nosonovsky, Contact modeling — Forces, Tribol. Int. 33 (5) (2000) 431–442, https://doi.org/10.1016/S0301-679X(00)00063-3.

[39] W. Dai, Y. Shi, Q. Wang, J. Wang, Smooth diamond-like carbon films prepared by cathodic vacuum arc deposition with large glancing angles, Diam. Relat. Mater. 141 (2024) 110672, https://doi.org/10.1016/j.diamond.2023.110672.

[40] H. Naragino, A. Tominaga, K. Hanada, T. Yoshitake, Synthesis method for ultrananocrystalline diamond in powder employing a coaxial arc plasma gun, Appl. Phys. Express. 8 (7) (2015), https://doi.org/10.7567/apex.8.075101.

[41] P. Panjan, A. Drnovšek, P. Gselman, M. Čekada, M. Panjan, Review of growth defects in thin films prepared by PVD techniques, Coatings 10 (5) (2020), https://doi.org/10.3390/coatings10050447.

[42] S. Zhang, C. Wang, Precise analysis of nanoparticle size distribution in TEM image, Methods Protoc. (2023), https://doi.org/10.3390/mps6040063.

[43] J. Ding, T. Zhang, H. Mei, J.M. Yun, S.H. Jeong, Q. Wang, K.H. Kim, Effects of negative bias voltage and ratio of nitrogen and argon on the structure and properties of NbN coatings deposited by HiPIMS deposition system, Coatings (2018), https://doi.org/10.3390/coatings8010010.

[44] Y. Chen, F. Su, H. Li, Q. Li, J. Sun, S. Lin, Hydrogen-free DLC films fabricated using superimposed HiPIMS-DCMS deposition system: bias voltage effects, Surf. Coat. Technol. 470 (2023) 129820, https://doi.org/10.1016/j.surfcoat.2023.129820.

[45] W. Xu, S. Lin, M. Dai, Q. Shi, C. Wei, X. Zhang, K. Zhou, Effects of bias voltage on the microstructure and properties of Al-doped hydrogenated amorphous carbon films synthesized by a hybrid deposition technique, Vacuum. 154 (2018) 159–166, https://doi.org/10.1016/j.vacuum.2018.05.008.

[46] A.C. Ferrari, J. Robertson, Raman spectroscopy of amorphous, nanostructured, diamond–like carbon, and nanodiamond, Philos. Trans. R. Soc. Lond. Ser. A: Math. Phys. Eng. Sci. 362 (1824) (2004) 2477–2512, https://doi.org/10.1098/rsta.2004.1452.

[47] H. Kuzmany, R. Pfeiffer, N. Salk, B. Günther, The mystery of the 1140 cm−1 Raman line in nanocrystalline diamond films, Carbon. N. Y. 42 (5–6) (2004) 911–917, https://doi.org/10.1016/j.carbon.2003.12.045.

[48] M. Egiza, M. Ragab Diab, H. Atta, M.M. Abdelfatah, A. El-Shaer, T. Yoshitake, Unveiling a 72.5 GPa peak hardness in sustainable nanodiamond composite hard coatings via discharge energy control: a nanoindentation-Raman approach, Mater. Lett. 369 (2024), https://doi.org/10.1016/j.matlet.2024.136684.

[49] A. van der Rest, H. Idrissi, F. Henry, A. Favache, D. Schryvers, J. Proost, J.-P. Raskin, Q. Van Overmeere, T. Pardoen, Mechanical behavior of ultrathin sputter deposited porous amorphous Al2O3 films, Acta Mater. 125 (2017) 27–37, https://doi.org/10.1016/j.actamat.2016.11.037.

[50] W. Tang, J.J. Yang, C.M. Li, Effect of film thickness and annealing time on residual stress of high-k Al2O3 film on Si- (100) substrate, Adv. Mat. Res. 644 (2013) 161–164, https://doi.org/10.4028/www.scientific.net/AMR.644.161.

[51] P. Pokorný, J. Musil, P. Fitl, M. Novotný, J. Lančok, J. Bulíř, Contamination of magnetron sputtered metallic films by oxygen from residual atmosphere in deposition chamber, Plasma Process. Polym. 12 (5) (2014) 416–421, https://doi.org/10.1002/ppap.201400172.

[52] S. Kumar, V.D. Mote, R. Prakash, V. Kumar, X-ray analysis of α-Al2O3 particles by Williamson–Hall methods, Mater. Focus 5 (6) (2016) 545–549, https://doi.org/10.1166/mat.2016.1345.

[53] A. Gaydaychuk, S. Linnik, Tribological and mechanical properties of diamond films synthesized with high methane concentration, Int. J. Refract. Metal. Hard Mater. 85 (2019) 105057, https://doi.org/10.1016/j.ijrmhm.2019.105057.

[54] P.K. Ajikumar, K. Ganesan, N. Kumar, T.R. Ravindran, S. Kalavathi, M. Kamruddin, Role of microstructure and structural disorder on tribological properties of polycrystalline diamond films, Appl. Surf. Sci. 469 (2019) 10–17, https://doi.org/10.1016/j.apsusc.2018.10.265.

[55] R. Rani, K.J. Sankaran, K. Panda, N. Kumar, K. Ganesan, S. Chakravarty, I.N. Lin, Tribofilm formation in ultrananocrystalline diamond film, Diam. Relat. Mater. 78 (2017) 12–23, https://doi.org/10.1016/j.diamond.2017.07.009.